Electrochimica Acta 55 (2010) 927–934

Contents lists available at ScienceDirect

Electrochimica Acta

journal homepage: www.elsevier.com/locate/electacta

Study of the storage performance of a Li-ion cell at elevated temperature

Jia Li*, Jian Zhang, Xigui Zhang, Chuanzheng Yang, Naixin Xu, Baojia Xia

Shanghai Institute of Microsystem and Information Technology, Chinese Academy of Sciences, No. 865 Changning Road, Shanghai, 200050, PR China

ARTICLE INFO

Article history:
Received 13 May 2009
Received in revised form
25 September 2009
Accepted 27 September 2009
Available online 4 October 2009

Keywords:
Li-ion cells
Storage
Safety
Microstructure
Impedance

ABSTRACT

A series of Li-ion cells with a $LiCoO_2$ cathode, artificial graphite anode and a $LiPF_6$-based nonaqueous electrolyte were stored at 55 °C in a series of state of charge (SoC) from 0 to 100%. After storage, all the cells except the one stored in 0% SoC exhibited capacity fade and cycling performance decline, which were aggravated by increasing storage SoC. Furthermore, storage at higher SoC increased the safety risk of the cells. The cells stored at SoC higher than 50% could not pass the 3 C/5 V overcharge test, while such a test was easy to pass for the fresh cells and those stored at 0% SoC. The above results show that the fully discharged state is a favorable storage condition to maintain good storage performance of Li-ion cells. In addition, to clarify the aging mechanisms of the cells, XRD (X-ray diffraction), SEM (scanning electron microscopy) and EIS (electrochemical impedance spectra) measurements were carried out. The results indicate that the performance fading of the stored cells is not due to the bulk structure change of the electrode materials, but instead due to the microstructure variation of the cathode, including the decrease in the crystallite dimension, the change of the micro-stress, and the precipitation of the surface films over the electrodes. According to EIS analysis, the increase of the cathode impedance may be the main contributor to the overall degradation of the Li-ion cells after storage.

1. Introduction

Due to the demonstrated advantages, including excellent energy density, high working potential, low self-discharge rate and outstanding long cycle life [1–3], Li-ion batteries have captured the commercial markets for powering high-end electronics applications such as portable phones, camcorders, computers, etc. Like other secondary batteries, Li-ion batteries are sometimes subjected to storage at various temperatures in practical applications. Therefore, storage performance is a crucial factor for Li-ion battery applications and many investigations are focused on this aspect [4–9]. Previous reports showed that storage at elevated temperature may cause damage to the batteries, and capacity decay and power fading always happen to the batteries during storage. Besides capacity, the degradation of cycling [10] and safety [11,12] performances are also important issues for Li-ion batteries, which cumber their practical applications especially in high power situations, such as electric vehicles (EV) and hybrid electric vehicles (HEV). Hitherto, few researchers have paid attention to the cyclability and safety variation after storage at elevated temperature, and no one has given a panorama of the performance deterioration of Li-ion batteries caused by thermal storage.

Additionally, aging mechanisms of Li-ion batteries have been investigated in the literature [13–21]. Some researchers have argued that the side-reaction on the cathode and the dissolution of the active materials [14–18] contribute to the capacity loss and increase in cell impedance [6,19]. Others have insisted that the anode is more responsible for the overall degradation of Li-ion batteries [5,20,21]. This ambiguity may lie in the fact that each Li-ion cell system has its own chemistry, and storage effects are influenced by the nature of the cell components (e.g., active materials, electrolyte composition, etc.), cell design, type of application and storage conditions, such as state of charge (SoC) [6,19,22].

In this paper, a type of Li-ion cell based on a $LiCoO_2$ cathode and artificial graphite anode in a $LiPF_6$-based nonaqueous electrolyte was stored at different SoC and elevated temperature. The performances, including capacity fading, charge–discharge behavior, cycling and safety before and after storage, were examined and compared to present a more complete scene of the ageing effect of Li-ion batteries. In order to clarify the contribution of each electrode to the overall degradation of the cells, the structure and surface morphology of the electrode materials before and after storage were investigated by X-ray diffraction (XRD) and scanning electron microscopy (SEM), and three-electrode electrochemical impedance spectroscopy (EIS) measurements were also performed.

2. Experimental

Storage tests were performed on rectangular, pouch cells with a nominal capacity of 1200 mAh and dimensions of 50 mm × 37 mm × 5 mm. The cell consists of (1) a cathode prepared

* Corresponding author. Tel.: +86 2162511070; fax: +86 2152419930.
E-mail address: lijia_miss@163.com (J. Li).

0013-4686/$ – see front matter © 2009 Elsevier Ltd. All rights reserved.
doi:10.1016/j.electacta.2009.09.077

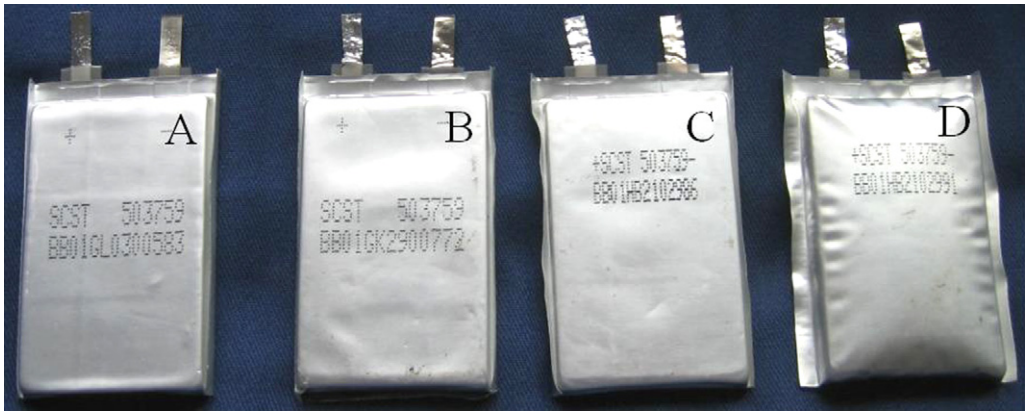

Fig. 1. Photographs of Li-ion cells after storage at 55 °C for 100 days. (a) Fresh cell; (b, c and d) cells stored in 0, 50 and 100% SoC, respectively.

by coating a slurry of $LiCoO_2$, super P black (SPB) and polyvinylidene difluoride (PVDF) in a weight ratio of 94:3:3 over an aluminum current collector (20 μm in thickness), (2) an anode prepared by coating a slurry of artificial graphite, SPB and styrene butadiene rubber (SBR) in a weight ratio of 92:4:4 over a copper current collector (15 μm in thickness), (3) a nonaqueous electrolyte containing a mixture of solvents, namely, ethylene carbonate (EC), dimethyl carbonate (DMC), diethyl carbonate (DEC) in a volume ratio of 1:1:1 and 1 M $LiPF_6$ dissolved in it, and (4) a separator (Celgard® 2320) of polypropylene/polyethylene/polypropylene with a thickness of 20 μm. The manufacturing process of the cells was as follows: the cathode and anode were pressed to resultant thicknesses of 140 and 130 μm, respectively. After drying at 120 °C for 4 h in a vacuum chamber, electrodes were cut into an appropriate size (50 mm × 37 mm) and stacked with a separator together in order of anode/separator/cathode/separator/anode/. . ./cathode. All cathodes were welded together with an aluminum lead as the cathode of the cell, and all anodes were connected with a nickel lead as the anode of the cell. The cell was then inserted into an aluminum-plastic film pouch. About 4.8 g of electrolyte were injected and the pouch was then sealed.

The charge and discharge tests were carried out on an Arbin BT-2401 battery instrument. Before storage, all fresh cells were cycled three times at room temperature (25 °C) in the following charge–discharge mode: a constant-current charge at a rate of 1 C (1200 mA) until a cut-off voltage of 4.20 V, then a constant-voltage charge at 4.20 V until a cut-off current with a rate of 0.01 C (12 mA), and finally a 30 min rest followed by a constant-current discharge at a rate of 1 C until a cut-off voltage of 2.75 V. The cells were then fully discharged (0% SoC), charged for 300, 600 and 900 mAh (25, 50 and 75% SoC), or fully charged (100% SoC), respectively, and stored in an open circuit state at 55 °C for 100 days.

The charge–discharge behavior and cycling performance of the fresh and stored cells were evaluated in the above charge–discharge mode at room temperature (25 °C). The safety performance was estimated by a 3 C/5 V overcharge test. In an airtight chamber, the fully charged cells were continuously charged in a procedure consisting of a constant-current at a rate of 3 C (3600 mA) until a cut-off voltage of 5 V followed by a constant-voltage charge at 5 V until the current tapered down to 0.01 C (12 mA) or the battery inflamed. During the test, the variation in temperature with time was recorded by an electronic digital recorder equipped with a thermocouple probe fixed tightly over the surface of the cells.

For further studies, some stored and fresh cells without any test were dismantled at the fully discharged state in a glove box filled with pure nitrogen. Both the positive $LiCoO_2$ and negative graphite electrodes were removed from the cell. Discs with a diameter of 1.2 cm were cut from the removed electrodes. The XRD measurements of electrode active materials were carried out on a Rigaku D/max2200PC diffractometer (Japan), and the surface morphology of the electrodes was observed using SEM (Shimadza, Japan). The samples were transported from the glove box to the analysis chambers using an inactive transfer vessel. For electrochemical measurements, three-electrode cells were assembled with a lithium disk and a lithium chip served as the counter and reference electrodes, respectively. The electrochemical impedance measurements were conducted by means of a Solartron Electrochemical Interface 1286 and Solartron FRA 1255 controlled by Zplot. The scanning frequency ranged from 10^5 to 10^{-2} Hz and the alternating voltage amplitude was set at 5 mV. The equivalent circuit fitting of the impedance data was done using the Zview software.

3. Results and discussion

3.1. Apparent characteristics

The appearance of the cells after storage in different SoC is shown in Fig. 1. The cell stored in a fully charged state (100% SoC) is bulging with gas, while ones stored in other SoC look almost the same as the fresh one. This shows that gas could be generated in the cell from some side-reactions of the electrodes with the electrolyte at elevated temperature. The extent would be more drastic for the cell stored in higher SoC. As shown in Table 1, in addition to an increase of the cell thickness, the open circuit voltage (OCV) drops after storage, while the internal resistance (IR) increases. The extents of these changes increased with increasing storage SoC.

3.2. Capacity and cycling performance

Fig. 2 shows the charge and discharge profiles of the cells before and after storage. It can be seen that a fresh cell has a capacity of 1227 mAh in the voltage range of 2.75–4.2 V at a rate of 0.2 C (240 mA). After storage, however, the capacities of the cells, except the one stored in 0% SoC, fade to various degrees. In particular, the cell stored in 100% SoC presents a capacity loss of almost 30%, while the cell stored in 0% SoC shows good capacity retention, and nearly has the same capacity as the fresh cell. This clearly reveals that the storage SoC plays an important role in the capacity fading effect in this system, and capacity loss seems to be a function of the storage SoC of the cells. Moreover, it can be seen from Fig. 2 that a negligible change in the charge-discharge voltage profile is observed for the cell stored in 0% SoC, even under prolonged storage, which indicates that it also exhibits excellent power retention, whereas the other stored cells suffer from a relatively higher build-up of polarization, which also seems to be affected by the

Table 1
Initial value and variations of OCV, IR and thickness of the cells after storage in different SoC.

Storage SoC (%)	OCV (V)		IR (mΩ)		Thickness (mm)	
	Initial	Δ	Initial	Δ	Initial	Δ
0	3.33	−0.38	20.1	1.20	4.89	0.03
25	3.75	−0.16	20.0	1.35	4.93	0.03
50	3.81	−0.02	19.9	2.50	4.98	0.04
75	3.94	−0.05	19.8	4.36	5.00	0.11
100	4.18	−0.10	19.8	9.50	5.02	0.67

Δ: variation of the values after storage.

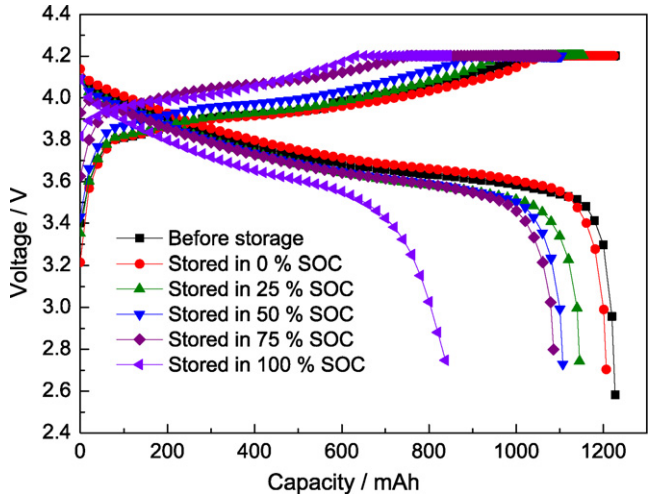

Fig. 2. Charge and discharge profiles at a rate of 0.2 C (240 mA) of the cells before and after storage in different SoC for 100 days.

storage SoC of the cells. Researchers proposed that increased cell polarization may result from changes in the electrodes ($LiCoO_2$ or graphite)/electrolyte interfacial characteristics, from increased internal ohmic resistance, or from changes in the lithium transport into the graphite bulk structure. This will be detailed in the following section on EIS measurements.

Fig. 3 compares the cycling performance of the cells during 100 cycles before and after storage. The cycling of a fresh cell is very stable with a less than 3% capacity loss after 100 cycles. Aside from the 0% SoC storage cell, the cells stored in other higher SoC show different cyclability declines after storage. This is especially the case for the cell stored at 100% SoC, whose capacity tails off most quickly as it loses approximately 25% of its initial capacity at the end of the cycling. Fig. 3 shows that storage in 0% SoC does not deteriorate the cycling characteristics of the cell. Hence, it could be concluded that high SoC storage impairs the cycling performance of the cells, and the impairing effect turns out to be more significant with increase of the storage SoC.

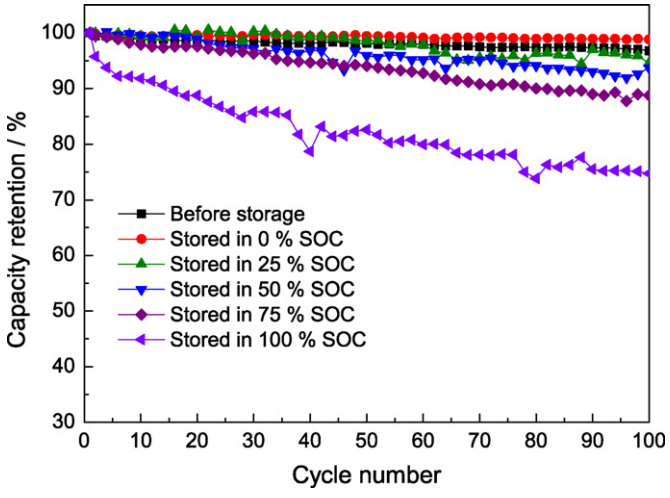

Fig. 3. Comparison of the cyclability of the fresh and stored cells.

3.3. Safety performance

The overcharge behavior of the cells before and after storage is presented in Fig. 4 and Table 2. According to our previous experiments, the fresh cell can pass this 3 C/5 V overcharge test easily with the surface temperature rising up to not more than 38 °C and then going down, as shown in Fig. 4(a). The cell stored in 0% SoC can also pass this overcharge test, and its overcharge curve is found to be nearly the same as that of the fresh one, as shown in Fig. 4(b), only with a slightly higher maximum temperature. However, for cells stored in higher SoC, the overcharge resistance is heavily reduced, which results in growing peak temperature and combustion of the cell, as presented in Table 2. A typical overcharge example of the cell stored in high SoC with a fire result is shown in Fig. 4(c). The entire overcharge process can be divided into four stages [23], namely A, B, C and D. In stage A, the cell temperature remained low for the first 13 min as the voltage rose to 5 V, and then the current began to decline gradually with constant voltage. In stages B and C, the cell temperature started to rise more rapidly, and the charging current stopped dropping and began to fluctuate. In stage D, the temperature rocketed to 180 °C in a very short time and the cell burst into flames. According to above phenomena, the stages can be further explained as follows [24]:

Stage A: Lithium is irreversibly removed from the Li_xCoO_2 cathode side and then deposited on the carbon anode. The cell voltage increases gradually with increasing delithiation of the cathode. The cell temperature remains low in this period.

Stage B: The cell temperature begins to rise rapidly due to the exothermic reaction between the electrodes and the electrolyte. The current fluctuation implies electrolyte decomposition. In the period of constant-voltage charge, normally without any side-reaction, the current drops gradually to the cut-off current as the amount of lithium delithiated from the cathode decreases, as shown in Fig. 4(a) and (b). However, if the electrolyte decomposes on the electrodes in this period, the reaction can give additional charge to add to the current, so the current stops dropping and begins to fluctuate.

Stage C: As the lithium deposits on the anode and the electrolyte is depleted, the cell impedance will increase. The cell case

Table 2
Results of 3 C/5 V overcharge test for cells after storage.

	0%SoC	25%SoC	50%SoC	75%SoC	100%SoC
Maximum temperature (°C)	42	58	180	195	213
Results	Pass	Pass	Fire	Fire	Fire

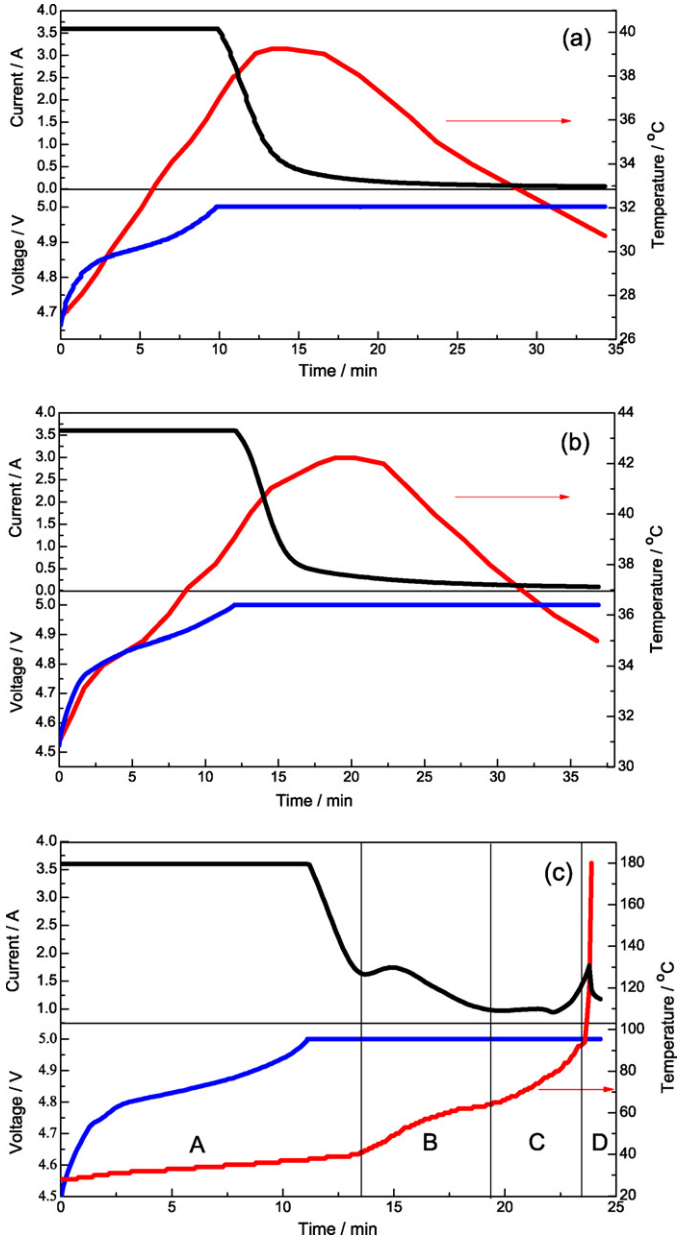

Fig. 4. Voltage, current and temperature of fresh cell (a), cells stored in 0% SoC (b) and 50% SoC (c) in the 3 C/5 V overcharge test.

temperature goes up due to the Joule heat. Meanwhile, the temperature rises high enough and exceeds the onset temperature of the SEI (solid electrolyte interphase) breakdown (60 °C). Thus, the SEI on the anode begins to decompose and the anode's passivation fails.

Stage D: Both the breakdown of SEI and the rise of the cell temperature lead to the violent reaction of the overcharged anode (deposited lithium) with the electrolyte. This reaction causes the temperature to increase sharply, thus resulting in the thermal runaway of the cell.

In a word, the difference between the overcharge behavior of the cell stored in low SoC and in high SoC can be attributed to the fact that the former does not experience stage B, where the reaction of the electrode with the electrolyte will lead to the temperature rise. It is known that an integrated SEI can passivate the anode and prevent it from reacting with the electrolyte. Therefore, it is demonstrated here that after high SoC storage the structure of SEI will be degenerated and the passivation of the anode will be partially lost.

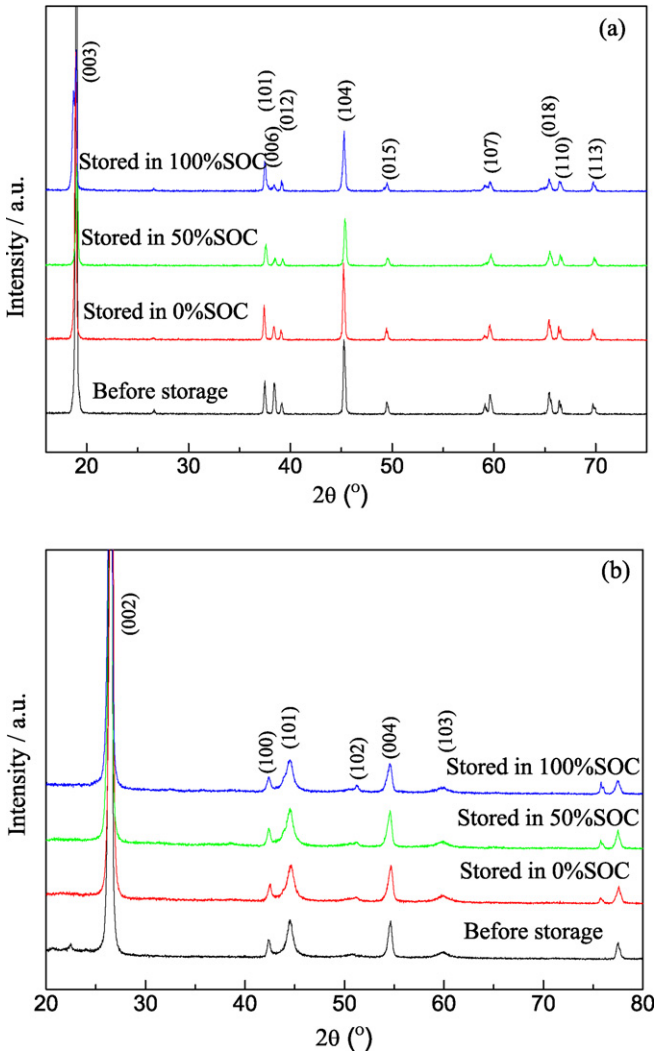

Fig. 5. XRD patterns for cathode (a) and anode (b) materials from the fresh and aged cells.

3.4. XRD measurement

In order to verify the crystal structure variation of the electrode materials after storage, XRD was performed on electrodes of the fresh and stored cells. Fig. 5 shows the XRD patterns of the cathode and anode materials of the cells. Samples for the XRD test were gained from the cells in their discharge state (2.75 V). All diffraction peaks of the stored samples are almost the same angular position as the fresh one, both for cathode and anode materials, with only slightly different relative intensities. Such differences in the relative intensities could not be clearly ascribed to phase transitions because they may also result from the electrode texture [25], which could vary during cycling and/or storage. The most significant change was found in the broadening of the peaks.

The full-width at half-maximum (FWHM) of the (0 0 3), (1 0 1) and (0 0 4) peaks for each cathode are presented in Table 3. The FWHM of the storage cathode are larger than that of the fresh one, and these larger amplitudes increase with increasing storage SoC, especially for the (0 0 3) peak. The broadening of the peaks may result from micro-stress within the crystallites, from a decrease in the dimension of the crystallite, and/or from an increase in the stacking faults [25]. Because there are no stacking faults in the crystal of $LiCoO_2$, the peak broadening of the cathodes may be caused by the micro-stress (ε) and the dimension of the crystallites

Table 3
FWHM of the (003), (101) and (004) peaks for each cathode material from the fresh and aged cells.

hkl		Fresh	Stored in 0%SoC	Stored in 50%SoC	Stored in 100%SoC
003	FWHM	0.134	0.161	0.206	0.364
101		0.146	0.148	0.196	0.173
004		0.153	0.154	0.195	0.204

(D). Previously, we have proposed a least square method for separating twofold broadening effects due to the crystallite-micro-stress, crystallite-stacking faults, micro-stress-stacking faults and the threefold effect of the crystallite-stress-faults, which has also been previously reported [26]. The D and ε can be calculated by the following equations:

$$\begin{cases} D = \dfrac{0.89\lambda}{\beta_{1/2}\cos\theta} = 0.89 \times \dfrac{n\sum X_i^2 - (\sum X_i)^2}{\sum Y_i \sum X_i^2 - \sum X_i \sum X_i Y_i} \\ \varepsilon = \dfrac{\beta_{1/2}\cot\theta}{4} = \dfrac{n\sum X_i Y_i - \sum X_i \sum Y_i}{n\sum X_i^2 - (\sum X_i)^2} \end{cases} \quad (1)$$

where

$$\begin{cases} Y_i = \dfrac{\beta_i \cos\theta_i}{\lambda} \\ X_i = \dfrac{4\sin\theta_i}{\lambda} \end{cases} \quad (2)$$

These apply for the case where there are n peaks used for the calculation. In the above equations, λ is the wavelength of X ray, and $\beta_{1/2}$ is the FWHM of each peak with the instrument broadening effect deducted. The results are presented in Table 4. Meanwhile, the lattice parameters a and c are calculated by means of the Calculate lattice and the Cell refinement options of Jade 6.5, also shown in Table 4. These reveal that, after storage, the lattice parameters of the cathode do not show a significant difference compared to the parameters of the fresh one, which suggests that the bulk phase of the cathode does not change. After storage, a trace of the delithiated hexagonal and the spinel phase may form on the grain surface [16,27], but because of the small amounts and the similar XRD patterns, XRD can hardly distinguish them from the bulk phase. From Table 4, it is clear that the broadening of the peaks could be attributed to the crystallite and the stress. The D of the stored cathodes is smaller than that of the fresh one, which decreases with increasing storage SoC. The micro-stress of the cathode changes from a tensile stress (positive value), as seen in the fresh one, to a compressive stress (negative value) after storage. The compressive stress increased with the increase of the storage SoC. Therefore, it is demonstrated that storage of the cathode does not consequentially lead to the bulk phase transition, but to significant modifications in the microstructure, including stress and crystallite.

By virtue of the similar methods to the data treatment of the cathode, the lattice parameter, D and ε for the anode are calculated and presented in Table 5. It should be pointed out that, unlike

Table 4
Lattice parameters, D and ε of cathode material from the fresh and aged cells after storage in different SoC.

	Fresh	Stored in 0%SoC	Stored in 50%SoC	Stored in 100%SoC
Lattice parameter (Å)				
a	2.8156	2.8126	2.8119	2.8123
c	14.0159	13.9975	13.9604	14.0072
Microstructure parameter				
D (nm)	336.1	116.9	67.2	19.4
ε ($\times 10^{-3}$)	0.269	−0.187	−0.352	−3.447

Table 5
Lattice parameters, D, ε and P of anode material from the fresh and aged cells in different SoC storages.

	Fresh	Stored in 0%SoC	Stored in 50%SoC	Stored in 100%SoC
Lattice parameter/Å				
a	2.4627	2.4538	2.4527	2.4517
c	6.7207	6.6960	6.7196	6.7219
Microstructure parameter				
D (nm)	52.9	75.7	111.8	65.8
ε ($\times 10^{-3}$)	0.983	2.350	2.404	2.400
P (%)	40.0	45.6	52.2	43.4

$LiCoO_2$, there are stacking faults (P) in the crystal of the graphite anode. These can be calculated by the following equation:

$$\frac{\beta_{101}\cos\theta_{101}}{\lambda} = \frac{\cos\theta_{101}}{2c} \cdot \frac{\cos\phi_{z101}}{\lambda} \cdot P + \varepsilon\frac{4\sin\theta_{101}}{\lambda} + \frac{0.89}{D} \quad (3)$$

where $\Phi_{z101} = 77.115^\circ$. Ignoring the minor difference of θ_{101} of the samples and with available data we can obtain:

$$0.6008\beta_{101} = 9.8061P + 0.9825\varepsilon + 0.89/D \quad (4)$$

where β_{101} is the FWHM of the (101) peak with the instrument broadening effect deducted. With the available D and ε, the P was calculated and is shown in Table 5. Combining almost the same XRD patterns and lattice parameters, it could be concluded that the bulk phase of the graphite anode does not change after storage. Meanwhile, except for the fact that ε that increases after storage, the crystallite and stacking faults do not vary as largely as the cathode does. This reveals that, compared to the anode, storage has a more significant effect on structure of the cathode, which may be associated with the performance degradation of the stored cells.

3.5. Surface morphology of the electrodes

Changes in the electrode interface after storage were studied carefully by observing scanning electron micrographs of the electrode surface. Fig. 6 presents the surface morphology of disassembled electrodes from the fresh and stored cells. As for the graphite anode, it is generally known that in the first charge the SEI films are formed on the surface of the anode, whose nature affects the performance of Li-ion cells [13]. From Fig. 6, it is obvious that there is a thin and uniform film appearing on the surface of the fresh anode (Fig. 6(a)), which is commonly considered as a SEI layer. After storage, the SEI morphology becomes much clearer, especially for the ones stored in higher SoC, which implies that its thickness augments with an increase of the storage SoC. Simultaneously, SEM images also indicate that after storage the SEI layer turned non-uniform, and they suggest the degradation of SEI, which may be one of the reasons for the cell performance deterioration. As for the cathode, almost no deposited film was observed on the fresh cell, but the deposited films were confirmed on the stored samples, whose appearance changed from having flecks (Fig. 6(f)) to protrusive (Fig. 6(g)) and squama-like (Fig. 6(h)) with increasing storage SoC. These surface films were reported to be formed by the deposition of electrolyte decomposition products [28]. It could be predicted that the amount of deposited substances on the surface increase as the storage SoC goes up.

Precipitation of surface films on the anode and cathode, which is intensified during high SoC storage, indicates that more film formation reactions occurred during storage and that the film formation consumes the Li-ions from the cathode and results in the decrease of the capacity of the cell. Additionally, the surface film may also increase the electrode's impedance because it negatively interferes with the inter-particle electrical contact, and hence, adds internal

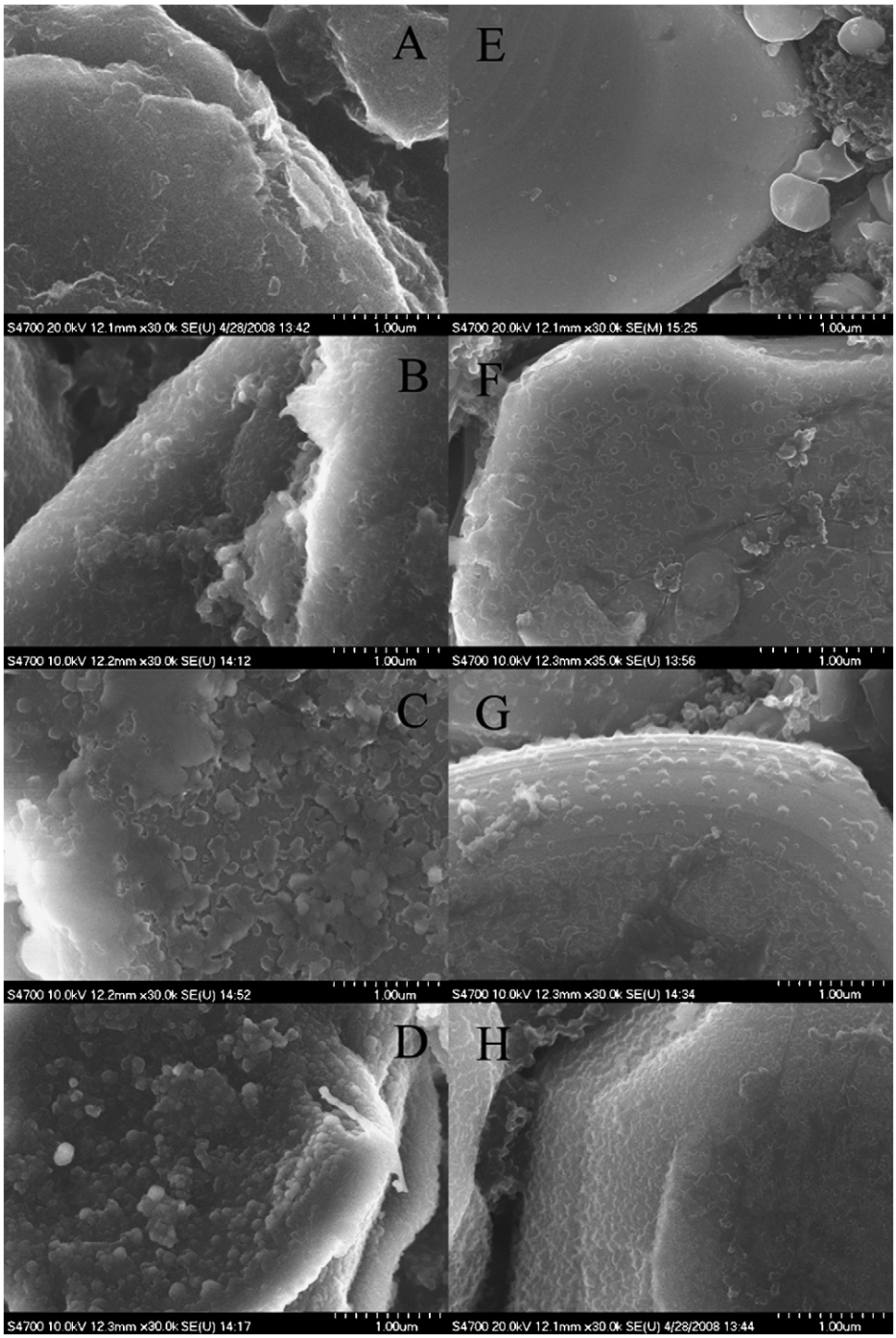

Fig. 6. SEM images of electrodes from the cells before and after storage. (a–d) The anodes of the fresh cell, the cells stored in 0% SoC, 50% SoC and 100% SoC, respectively; (e–h) the cathodes likewise.

impedance and problems of electrical contact between the active mass and the current collector [29].

3.6. EIS analysis

Fig. 7 shows the Nyquist plots for the disassembled electrodes before and after storage. The impedance of the stored graphite anodes is larger than that of the fresh one, which increases with the increase of the storage SoC. The Nyquist plots are composed of two partially overlapped semicircles at high and medium frequencies and a straight slopping line at low frequency. Such an EIS plot can be fitted by an equivalent circuit as shown in Fig. 8(a). Here, *Re* is the ohmic resistance, which is a combined resistance of the electrolyte and separator. R_{SEI} and CPE_1 are the resistance and imperfect capacitance of the SEI, which correspond to the semicircle at high frequencies. R_{CT} and CPE_2 are the charge-transfer resistance and its relative double-layer capacitance, which correspond to the semicircle at medium frequencies. CPE_3 is the electrode limit capacitance (CL) related to the solid-state lithium ion diffusion within the electrode [30] that could be detected by the inclined straight line towards the real axes at low frequency. A constant phase element (CPE) is used here to simulate the rough and porous surface of the

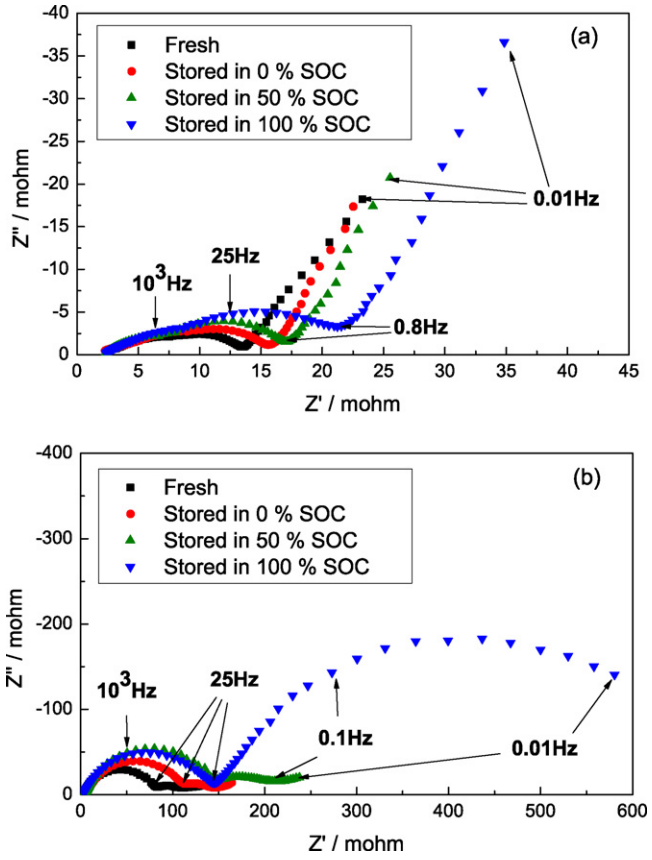

Fig. 7. Nyquist plots for disassembled anodes (a) and cathodes (b) from the cells before and after storage.

electrode. The R_{SEI} and R_{CT} of the anodes stored in different SoC are presented in Fig. 9. It is shown that both the SEI film resistance and charge-transfer resistance of the anode increase after storage, and the higher storage SoC enhances their accretion. By careful inspection of SEM, it is known that, during storage, more new SEI film would be formed on the anode surface, resulting in the increase of the thickness of SEI, which might be the reason for the impedance rise of the anode [29].

As shown in Fig. 7(b), the impedance of the $LiCoO_2$ cathode also increased after storage. The cathode stored in 100% SoC showed the greatest increase in impedance. The equivalent circuit used for fitting the cathode impedance is shown in Fig. 8(b). Here, R_f and CPE_1 are the surface film resistance and its corresponding imperfect capacitance. W is the Warburg impedance related to the solid-state Li-ion diffusion in the electrode, which corresponds to the straight sloping line at low frequency. Other elements have the same meaning in the equivalent circuit for the anode. The simulation results are also presented in Fig. 9. It could be seen that, compared to the SEI film, the surface film on the cathode shows a much higher resistance and increases after storage. It also shows that, after storage in 100% SoC, the R_{CT} increases dramatically to a value where a semicircle cannot be drawn completely in Fig. 7(b). Aurbach et al. [12,15] considered the precipitated LiF as the most likely major contributor to a high resistance layer on the cathode. More details will be discussed in next section.

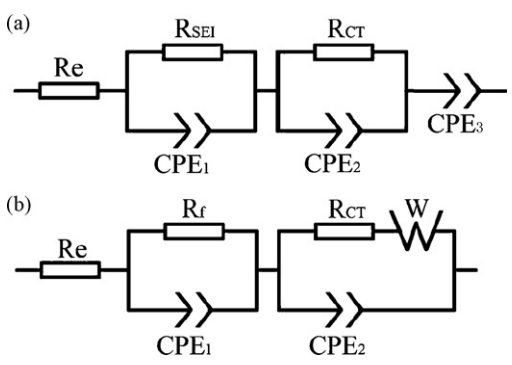

Fig. 8. Equivalent circuits for (a) the anode and (b) the cathode.

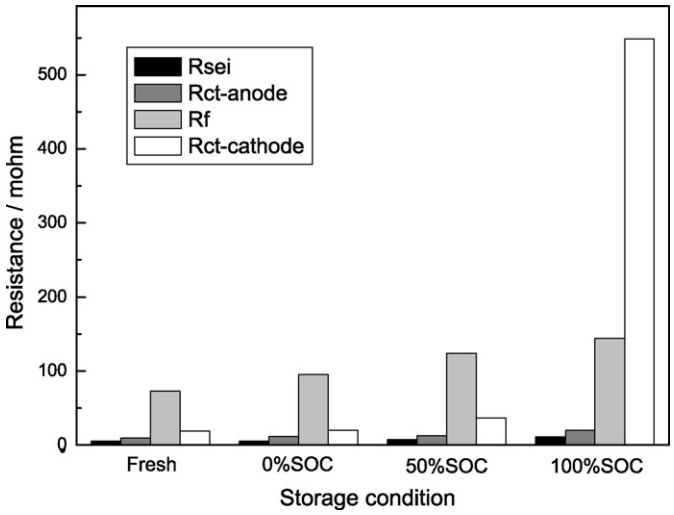

Fig. 9. Simulation results of EIS for the electrodes disassembled from the cells before and after storage in different SoC.

4. Discussion

Based on the above experimental results, it can be concluded that the performance of Li-ion cells deteriorates after the cells are stored in high SoC, and the variation of the surface chemistry of the electrodes, especially of the cathode, may contribute to the degradation of the cells after storage. The possible degradation mechanisms for the electrodes in high SoC can be explained as follows:

4.1. Degradation mechanisms for the cathode

Firstly, in the charge–discharge process of $LiCoO_2$-based Li-ion cells between 4.2 and 2.75 V, the cathode stoichiometry varies between $LiCoO_2$ and $Li_{0.5}CoO_2$ in the fully discharged and charged states, respectively. It has been shown that the cohesive energy of the crystal is heightened by the extraction of Li cations from the $LiCoO_2$ crystal [31], and the structure of $Li_{1-x}CoO_2$ starts to deteriorate when the cell is charged to 4.20 V ($Li_{0.5}CoO_2$) [17]. The charged $Li_{1-x}CoO_2$ ($0 < x < 0.5$) is acknowledged as metastable [32] compared with the discharged $LiCoO_2$. Hence, when the cell is stored in high SoC, due to the instability, the surface $Li_{1-x}CoO_2$ decomposes to form the stable $LiCoO_2$, and the following reaction takes place:

$$Li_{1-x}CoO_2 \rightarrow (1-x)\,LiCoO_2 + \frac{x}{3}CoO_2 + \frac{x}{3}Co_2O_3 + \frac{x}{6}O_2 \qquad (1)$$

This may lead to modifications in the microstructure including stress and crystallite on the cathode, as shown in Table 4, and to a loss of active material and therefore capacity fading. Due to the oxidizing ability of the cobalt oxide ($Co^{IV}O_2$, $Co^{III}{}_2O_3$), the Co^{4+} and Co^{3+} oxidize solvent molecules [14] and are themselves reduced to Co^{2+}, which easily dissolves in solution [33]. Meanwhile, the evolved oxygen can also oxidize solvent molecules. The oxidation products precipitate on the cathode forming a thick surface film (seen in Fig. 6).

Secondly, as the SoC of the cell increase, the potential of the cathode also increases. The OCV of Li-ion batteries in their fully charged state (SoC = 100%) is around 4.2 V, indicating a potential of the $Li_{1-x}CoO_2$ electrode higher than 4.2 V vs. Li/Li^+. Although the electrochemical window of the electrolyte of the Li-ion cells is wider than 5 V, the electrolyte can be oxidized at a very small rate at a potential lower than 4 V. When the cells are stored in high SoC, the electrolyte can be slowly oxidized on the cathode at high potential, and the products deposit on the electrode leading to the increment of the surface film.

Finally, it is found that pristine $LiCoO_2$ powder always contains Li_2CO_3 on the surface [34], which contributes to the high *Rf* of the fresh cathode in Fig. 9. During elevated temperature storage, $LiPF_6$ undergoes thermal decomposition to generate PF_3O and HF [35]. The superficial Li_2CO_3 can also react with HF to form LiF [16]. The reactions can be written as follows:

$$LiPF_6 \rightarrow LiF + PF_5 \quad (2)$$

$$PF_5 + H_2O \rightarrow PF_3O + 2HF \quad (3)$$

$$Li_2CO_3 + 2HF \rightarrow 2LiF + H_2O + CO_2 \quad (4)$$

It is likely that the products of such reactions congregate on the cathode surface at a faster rate in high SoC. As a result, the total thickness of the surface film increases quickly. It should be noted that LiF films are highly resistive [15]. Precipitation of LiF could affect ionic motion by pore plugging, or could contribute to electrical resistive paths to parts of the cathode structure, so that the active mass seems to be blocked for the possible Li ion insertion [29].

Hence, the increment of the surface film on the cathode increases the electrodes' impedance, leading to the apparent capacity fading observed for Li-ion cells after storage in high SoC.

4.2. Degradation mechanisms for the anode

The lithiated graphite is also considered to be unstable because the intercalated lithium tends to diffuse to the graphite edges driven by the chemical potential [36]. On the edges of the graphite, due to the high reactive activity of lithium with the solvent, lithium may release an electron turning into Li^+ entering the electrolyte, and the electron transfers to the solvent leading to subsequent decomposition (Li–C + solvent → Li^+ + C + solvent•). The SEI on the anode increases in thickness with the deposition of decomposition products, which may also increase the impedance as seen in Fig. 7(a). However, its contribution to the degradation of the cell seems much smaller than that of the cathode.

5. Conclusions

The storage performance of a $LiCoO_2$/graphite Li-ion cell has been studied in detail. Storage SoC plays an important part in the aging effect of the cells. High SoC storage, especially for the fully charged state, augments the capacity fading and the polarization in the charge–discharge process, and it deteriorates the cycling performance of the cells. The impairing effect turns out to be more significant with increasing SoC. In addition, the overcharge resistance of the cells degrades after storage at elevated temperature. The cells stored in SoC higher than 50% could not pass the 3 C/5 V overcharge test. Among the aged cells, the cell stored in 0% SoC exhibits almost no performance decline, and so the fully discharged state is a favorable condition to maintain good storage performance of Li-ion cells. In order to clarify the reasons for the performance degradation during high SoC storage, the cells were disassembled, and XRD, SEM and EIS measurements of the electrodes were carried out. The results indicate that the bulk structures of both electrode materials do not change after storage, and the increased performance fading for the cells stored in higher SoC could be attributed to the microstructure variation of the cathode, including the decrease of the crystallite dimension and the change of the micro-stress, and the precipitation of the surface films over the electrodes, which results in the increased Li-ion consumption and also in the rise of the electrodes' impedance. The EIS analysis shows that, compared to the SEI films over the anode, the surface films on the cathode show a much higher resistance, and the increase of the cathode impedance may contribute to the overall degradation of the Li-ion cells after storage.

Acknowledgments

The authors would like to acknowledge the support from the National Natural Science Foundation of China (Grant No. 20773157) and the Project of Excellent Academic Pacemaker of Shanghai (Grant No. 07XD14035).

References

[1] D. Aurbach, Y. Gofer, Z. Lu, A. Schechter, O. Chusid, H. Gizbar, Y. Cohen, V. Ashkenazi, M. Moshkovich, R. Turgeman, E. Levi, J. Power Sources 97–98 (2001) 28.
[2] J.F. Coussea, C. Siret, P. Biensan, M. Broussely, J. Power Sources 162 (2006) 790.
[3] W.Y. Liu, Z.W. Fu, Q.Z. Qin, J. Electrochem. Soc. 155 (2008) A8.
[4] K. Amine, J. Liu, I. Belharouak, Electrochem. Commun. 7 (2005) 669.
[5] R.P. Ramasamy, J.W. Lee, B.N. Popov, J. Power Sources 166 (2007) 266.
[6] C. Huang, K. Huang, S. Liu, Y. Zeng, L. Chen, Electrochim. Acta 54 (2009) 4783.
[7] B. Markovsky, Y. Talyossef, G. Salitra, D. Aurbach, H.J. Kim, S. Choi, Electrochem. Commun. 6 (2004) 821.
[8] Q. Zhang, R.E. White, J. Power Sources 179 (2008) 793.
[9] D. Aurbach, B. Markovsky, A. Rodkin, M. Cojocaru, E. Levi, H.J. Kim, Electrochim. Acta 47 (2002) 1899.
[10] R.A. Leising, M.J. Palazzo, E.S. Takeuchi, K.J. Takeuchi, J. Electrochem. Soc. 148 (2001) A838.
[11] P.G. Balakrishnan, R. Ramesh, T.P. Kumar, J. Power Sources 155 (2006) 401.
[12] D. Aurbach, B. Markovsky, G. Salitra, E. Markevich, Y. Talyossef, M. Koltypin, L. Nazar, B. Ellis, D. Kovacheva, J. Power Sources 165 (2007) 491.
[13] M. Broussely, P. Biensan, F. Bonhomme, P. Blanchard, S. Herreyre, K. Nechev, R.J. Staniewicz, J. Power Sources 146 (2005) 90.
[14] Z.X. Wang, L.Q. Chen, J. Power Sources 146 (2005) 254.
[15] D. Aurbach, B. Markovsky, A. Rodkin, E. Levi, Y.S. Cohen, H.J. Kim, M. Schmidt, Electrochim. Acta 47 (2002) 4291.
[16] K. Edstrom, T. Gustafsson, J.O. Thomas, Electrochim. Acta 50 (2004) 397.
[17] G.G. Amatucci, J.M. Tarascon, L.C. Klein, Solid State Ionics 83 (1996) 167.
[18] E. Markevich, G. Salitra, D. Aurbach, Electrochem. Commun. 7 (2005) 1298.
[19] D.P. Abraham, S.D. Poppen, A.N. Jansen, J. Liu, D.W. Dees, Electrochim. Acta 49 (2004) 4763.
[20] L.J. Fu, K. Endo, K. Sekine, T. Takamura, Y.P. Wu, H.Q. Wu, J. Power Sources 162 (2006) 663.
[21] G. Kwak, J. Park, J. Lee, S. Kim, I. Jung, J. Power Sources 174 (2007) 484.
[22] Y.B. He, Z.Y. Tang, Q.S. Song, H. Xie, Q. Xua, Y.G. Liu, G.W. Ling, Thermochim. Acta 480 (2008) 15.
[23] Y.Q. Zeng, K. Wu, D.Y. Wang, Z.X. Wang, L.Q. Chen, J. Power Sources 160 (2006) 1302.
[24] T. Ohsaki, T. Kishi, T. Kuboki, N. Takami, N. Shimura, Y. Sato, M. Sekino, A. Satoh, J. Power Sources 146 (2005) 97.
[25] Y. Ozawa, R. Yazami, B. Fultz, J. Power Sources 119–121 (2003) 918.
[26] P. Qin, Y.W. Lou, C.Z. Yang, B.J. Xia, Acta Phys. Sin. 55 (2006) 1325.
[27] H. Gabrisch, Y. Ozawa, R. Yazami, Electrochim. Acta 52 (2006) 1499.
[28] W.T. Li, B.L. Lucht, J. Power Sources 168 (2007) 258.
[29] D. Aurbach, B. Markovsky, I. Weissman, E. Levi, Y. Ein-Eli, Electrochim. Acta 45 (1999) 67.
[30] J.R. MacDonald, Impedance Spectroscopy, John Wiley & Sons Editor, New York, 1987.
[31] H. Gabrisch, R. Yazami, B. Fultz, J. Electrochem. Soc. 151 (2004) A891.
[32] Y. Baba, S. Okada, J. Yamaki, Solid State Ionics 148 (2002) 311.
[33] M.S. Wu, P.C. Julia Chiang, J.C. Lin, J. Electrochem. Soc. 152 (2005) A1041.
[34] H.S. Liu, Y. Yang, J.J. Zhang, J. Power Sources 162 (2006) 644.
[35] H. Yang, G.V. Zhuang, P.N. Ross Jr., J. Power Sources 161 (2006) 573.
[36] R. Yazami, Y.F. Reynier, Electrochim. Acta 47 (2002) 1217.